IEEE Access
Multidisciplinary | Rapid Review | Open Access Journal

Received November 7, 2020, accepted November 19, 2020, date of publication December 14, 2020,
date of current version January 13, 2021.

Digital Object Identifier 10.1109/ACCESS.2020.3044871

Analytical Expressions for the Magnetic Field Generated by a Circular Arc Filament Carrying a Direct Current

MIGDONIO ALBERTO GONZÁLEZ, (Member, IEEE), AND DORINDO ELÁM CÁRDENAS, (Senior Member, IEEE)
School of Electrical Engineering, Universidad Tecnológica de Panamá, Panama City 0819-07289, Panama

Corresponding author: Migdonio Alberto González (migdonio.gonzalez@utp.ac.pa)

This work was supported by the SENACYT through the SNI program and by the Universidad Tecnológica de Panamá through the Centro de Estudios Multidisciplinarios en Ciencias, Ingeniería y Tecnología AIP (CEMCIT-AIP) and ERDI Research Laboratory.

ABSTRACT This paper presents a simple, didactical and compact solution for the components of the magnetic vector potential and magnetic field generated by a circular arc filament carrying a direct current using the well-known incomplete elliptic integrals, their properties and formulas. Using a well-defined method, the expressions are obtained in Cartesian coordinates and then easily transformed to a compact expression in cylindrical coordinates. The paper provides numerical data for different study cases where arbitrary arc filaments are considered. Through Gauss' magnetic law, special cases, and comparisons with numerical methods, a degree of validation is provided for the derived expressions.These solutions represent a computational advantage for magnetic field calculations for applications like wireless power transfer. Finally, new integral formulas are derived using elliptic integrals.

INDEX TERMS Circular arc filament, elliptic integrals, Jacobi elliptic functions, magnetic field, wireless power transfer.

I. INTRODUCTION

The interest for wireless power transfer (WPT) using magnetic coupling in different common applications has been booming since the Massachusetts Institute of Technology (MIT) developed a highly efficient WPT resonant system in 2007 [1]. These applications include wireless power transmission systems for wireless charging of cellular phones [2]–[4], electric vehicles [5], [6], and medical equipment [7]–[9]. Every day, we find new applications, including underwater applications [10] and space applications [11]. For wireless power transmission resonant systems, the ability to measure or predict the magnetic coupling between the coils of the system is fundamental, and having expressions to compute the magnetic field generated by the coils is very useful.

In wireless power transfer applications via magnetic coupling, we may find different geometries for the coils of the system. The cylindrical coil, for example, is a common geometry that can be studied as a series of circular loops. For a circular loop carrying a direct current, expressions for the magnetic field in the loop's axis are well known and are derived in any electromagnetics textbook [12], [13]. General expressions for the magnetic vector potential and magnetic field vector outside the loop's axis have been derived using complete elliptic integrals [14]. Other books have derived partial and complete closed-form expressions for the same problem [15], [16]. To verify the expressions in the mentioned articles and textbooks, the general expressions are reduced to known special cases and the resulting expressions are compared with the known formulas for the magnetic field. In the literature, Gauss's magnetic law has been used to verify self-consistency of the mathematical expressions [17].

In the present literature, analytical solutions for the circular loop problem exist, but only a small part of the literature focuses on deriving expressions for an arbitrarily shaped arc filament. A series of papers have derived analytical expressions for a finite arc segment of a filament and other cross sections [18]–[21]. The expressions derived in these papers are written in terms of Jacobian elliptic functions and elliptic

The associate editor coordinating the review of this manuscript and approving it for publication was Xiaokang Yin.

integrals. These kinds of expressions are specially useful because we can usually break down complex geometries into simple shapes. None of these efforts have: 1.) derived analytical expressions for the magnetic vector potential and magnetic field vector of circular arc filaments carrying a direct current using only elliptic integrals, 2.) defined a didactical method to solving these magnetic field integrals and 3.) offered numerical study cases for filaments with different geometrical properties.

In this paper, we derive expressions for the magnetic vector potential and magnetic field vector using incomplete elliptic integrals, and we present several integral formulas useful for magnetic field problems concerning cylindrical geometries. We check the validity of the expressions by assuming that the filament is a circular loop and then comparing with the known formulas for the magnetic field generated by a circular loop carrying a direct current. Gauss's magnetic law is also used to show self-consistency of the equations. This analysis is for the computation of quasi-static magnetic fields and it does not apply for cases such as loop antennas and EM radiation.

We organize the paper as follows. In section II, we describe the geometry of the problem and through Biot-Savart law's equation and magnetic vector potential equations we establish the mathematical problem. In section III, we derive expressions for the magnetic vector potential in cylindrical coordinates using incomplete elliptic integrals. In section IV, we derive expressions for the magnetic field vector in cylindrical coordinates using incomplete elliptic integrals and we show self-consistency using Gauss's magnetic law. We focus section V on the reduction of the expressions for a circular loop special case. In section VI we present several numerical study cases that include magnetic field plots and numerical values at different test points. Finally, in section VII we validate the derived expressions by comparing numerical results from the formulas with the numerical results obtained from a numerical integration method.

II. PROBLEM FORMULATION

In this work, we use a Cartesian coordinates system with orthogonal axes x, y and z. The orthogonal unit vectors for the Cartesian coordinates system are $\boldsymbol{e}_x$, $\boldsymbol{e}_y$ and $\boldsymbol{e}_z$. For convenience, we will make use of a cylindrical coordinates system with orthogonal axes ρ, ϕ and z. The orthogonal unit vectors for the cylindrical coordinates system are $\boldsymbol{e}_\rho$, $\boldsymbol{e}_\phi$ and $\boldsymbol{e}_z$.

Let us consider a circular arc filament that carries a direct current I. We assume that the surroundings of the filament have properties very similar to free-space. The coordinates of any point on the filament, in a cylindrical coordinates system, are (ρ', ϕ', z') which are correlated with Cartesian coordinates (x', y', z'). The filament goes from $\phi = \phi_1$ to $\phi = \phi_2$. The $z-$ axis is the turning axis of the circular arc. See Figure 1. We place an arbitrary test point in space with coordinates (ρ, ϕ, z) as shown. Our goal is to derive a general expression for the magnetic field at the test point. We start by defining a vector $\boldsymbol{\xi}$ that goes from any point on the filament

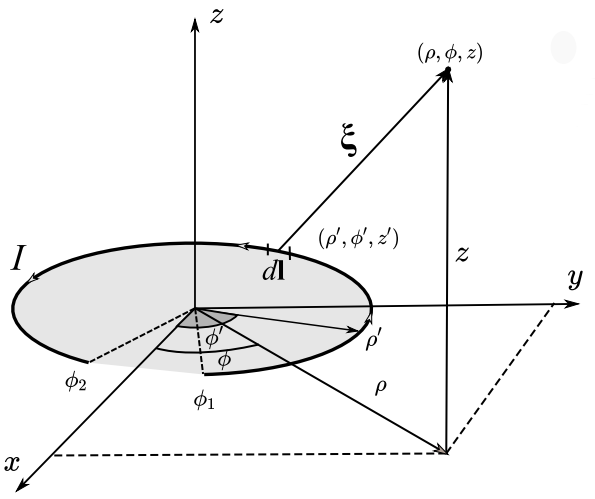

FIGURE 1. Circular arc filament of radius ρ' going from $\phi = \phi_1$ to $\phi = \phi_2$. The filament carries a direct current I.

to the test point in space:

$$\boldsymbol{\xi} = (x - x')\boldsymbol{e}_x + (y - y')\boldsymbol{e}_y + (z - z')\boldsymbol{e}_z$$

It will be useful for our purposes to transform the Cartesian coordinates values to cylindrical coordinates values by applying the relations $x' = \rho' \cos(\phi')$, $y' = \rho' \sin(\phi')$, $x = \rho \cos(\phi)$ and $y = \rho \sin(\phi)$:

$$\begin{aligned}\boldsymbol{\xi} &= [\rho \cos(\phi) - \rho' \cos(\phi')]\boldsymbol{e}_x \\ &\quad + \left[\rho \sin(\phi) - \rho' \sin(\phi')\right]\boldsymbol{e}_y + (z - z')\boldsymbol{e}_z \end{aligned} \tag{1}$$

From this expression, we can find an expression for the norm of the vector ξ (some trigonometric simplifications are required):

$$\xi^2 = \rho'^2 + \rho^2 + (z - z')^2 - 2\rho'\rho \cos(\phi' - \phi) \tag{2}$$

The differential line element along the arc is given by:

$$\begin{aligned} d\boldsymbol{l} &= \rho' d\phi' \boldsymbol{e}_\phi \\ d\boldsymbol{l} &= \rho' d\phi' [-\sin(\phi')\boldsymbol{e}_x + \cos(\phi')\boldsymbol{e}_y] \end{aligned} \tag{3}$$

We compute the cross product $d\boldsymbol{l} \times \boldsymbol{\xi}$:

$$\begin{aligned} d\boldsymbol{l} \times \boldsymbol{\xi} &= \rho' d\phi' \{[(z - z')\cos(\phi')]\boldsymbol{e}_x + [(z - z')\sin(\phi')]\boldsymbol{e}_y \\ &\quad + \left[\rho' - \rho \cos(\phi' - \phi)\right]\boldsymbol{e}_z\} \end{aligned} \tag{4}$$

Using Biot-Savart law, the equation for magnetic vector potential and equations (1), (2) and (4), we obtain expressions for the magnetic vector potential $\boldsymbol{A}(\rho, \phi, z)$ and the magnetic field vector $\boldsymbol{B}(\rho, \phi, z)$. The expression for the magnetic vector potential is given by:

$$\begin{aligned} \boldsymbol{A}(\rho, \phi, z) &= \frac{\mu_0}{4\pi} \int_{\phi_1}^{\phi_2} \frac{I d\boldsymbol{l}}{\xi} \\ \boldsymbol{A}(\rho, \phi, z) &= \frac{\mu_0 I \rho'}{4\pi} \int_{\phi_1}^{\phi_2} \frac{[-\sin(\phi')\boldsymbol{e}_x + \cos(\phi')\boldsymbol{e}_y]}{\xi} d\phi' \end{aligned} \tag{5}$$

Here ξ is given by equation (2). The expression for the magnetic field vector is given by:

$$\boldsymbol{B}(\rho,\phi,z) = \frac{\mu_0}{4\pi}\int_{\phi_1}^{\phi_2}\frac{Id\boldsymbol{l}\times\boldsymbol{\xi}}{\xi^3}$$

$$\begin{aligned}\boldsymbol{B}(\rho,\phi,z) = \frac{\mu_0 I\rho'}{4\pi}\int_{\phi_1}^{\phi_2}\frac{1}{\xi^3}\cdot\Big\{&[(z-z')\cos(\phi')]\boldsymbol{e}_x\\ &+\left[(z-z')\sin(\phi')\right]\boldsymbol{e}_y\\ &+[\rho'-\rho\cos(\phi'-\phi)]\boldsymbol{e}_z\Big\}d\phi'\end{aligned} \tag{6}$$

Here ξ is given by equation (2). Simple analytical solutions can be obtained for equation (5) and equation (6) in terms of elliptic integrals. These expressions will be obtained in the next sections using simple methods.

III. ANALYTICAL EXPRESSIONS FOR THE COMPONENTS OF THE MAGNETIC VECTOR POTENTIAL

Let us express the magnetic vector potential in equation (5) as:

$$\boldsymbol{A}(\rho,\phi,z) = \frac{\mu_0 I\rho'}{4\pi}(A_x\boldsymbol{e}_x + A_y\boldsymbol{e}_y) \tag{7}$$

where A_x and A_y are:

$$A_x = -\int_{\phi_1}^{\phi_2}\frac{\sin(\phi')d\phi'}{\sqrt{\rho'^2+\rho^2+(z-z')^2-2\rho'\rho\cos(\phi'-\phi)}} \tag{8}$$

$$A_y = \int_{\phi_1}^{\phi_2}\frac{\cos(\phi')d\phi'}{\sqrt{\rho'^2+\rho^2+(z-z')^2-2\rho'\rho\cos(\phi'-\phi)}} \tag{9}$$

In this section we'll find an analytical solution using elliptic integrals to solve the integrals in equation (8) and equation (9). Both integrals can be reduced to the similar forms. For this reason, we'll make use of the following solved integrals:

$$\int_{\phi_1}^{\phi_2}\frac{\sin(\phi'-\phi)d\phi'}{\sqrt{a-b\cos(\phi'-\phi)}} = \frac{2\sqrt{a-b\cos(\phi'-\phi)}}{b}\Bigg|_{\phi_1}^{\phi_2} \tag{10}$$

$$\begin{aligned}\int_{\phi_1}^{\phi_2}\frac{\cos(\phi'-\phi)d\phi'}{\sqrt{a-b\cos(\phi'-\phi)}} &= \frac{2a}{b\sqrt{a+b}}\mathrm{F}\left(\frac{\phi'-\phi-\pi}{2},\frac{2b}{a+b}\right)\\ &\quad-\frac{2\sqrt{a+b}}{b}\mathrm{E}\left(\frac{\phi'-\phi-\pi}{2},\frac{2b}{a+b}\right)\Bigg|_{\phi_1}^{\phi_2}\end{aligned} \tag{11}$$

The proofs of these formulas are shown in the appendix of this article due to lengthy procedure. Here a and b are constants and F and E are incomplete elliptic integrals of the first and second kind, respectively. Let us focus first on the integral in equation (8). We start by doing some basic algebraic manipulations:

$$-\int_{\phi_1}^{\phi_2}\frac{\sin(\phi')d\phi'}{\sqrt{\rho'^2+\rho^2+(z-z')^2-2\rho'\rho\cos(\phi'-\phi)}}$$

$$= -\int_{\phi_1}^{\phi_2}\frac{\sin(\phi'-\phi+\phi)d\phi'}{\sqrt{\rho'^2+\rho^2+(z-z')^2-2\rho'\rho\cos(\phi'-\phi)}}$$

We now use the angle sum trigonometric identity:

$$\begin{aligned}&-\int_{\phi_1}^{\phi_2}\frac{\sin(\phi'-\phi+\phi)d\phi'}{\sqrt{\rho'^2+\rho^2+(z-z')^2-2\rho'\rho\cos(\phi'-\phi)}}\\ &= -\int_{\phi_1}^{\phi_2}\frac{[\sin(\phi'-\phi)\cos(\phi)+\cos(\phi'-\phi)\sin(\phi)]d\phi'}{\sqrt{\rho'^2+\rho^2+(z-z')^2-2\rho'\rho\cos(\phi'-\phi)}}\end{aligned}$$

This integral has the form of the integrals described in the formulas (10) and (11). We now apply the formulas with $a = \rho'^2+\rho^2+(z-z')^2$ and $b = 2\rho'\rho$:

$$A_x = -\frac{1}{\rho'\rho}\left[\cos(\phi)f_1(\phi')+\sin(\phi)f_2(\phi')\right]\Big|_{\phi_1}^{\phi_2} \tag{12}$$

The functions f_1 and f_2 are used to reduce the length of the expressions and are useful for computational purposes. These functions are defined as:

$$f_1(\phi') = \sqrt{\rho'^2+\rho^2+(z-z')^2-2\rho'\rho\cos(\phi'-\phi)} \tag{13}$$

$$\begin{aligned}f_2(\phi') = \frac{\rho'^2+\rho^2+(z-z')^2}{\sqrt{(\rho'+\rho)^2+(z-z')^2}}\mathrm{F}\left(\frac{\phi'-\phi-\pi}{2},m\right)\\ -\sqrt{(\rho'+\rho)^2+(z-z')^2}\mathrm{E}\left(\frac{\phi'-\phi-\pi}{2},m\right)\end{aligned} \tag{14}$$

Here, the parameter m is defined as:

$$m = \frac{4\rho'\rho}{(\rho'+\rho)^2+(z-z')^2} \tag{15}$$

The parameter m will take values between 0 and 1 for real positive values of ρ', ρ, z' and z. Now we focus on the integral in equation (9). Using a similar procedure and using equations (13) and (14) we find an expression for the integral in (9):

$$A_y = \frac{1}{\rho'\rho}\left[\cos(\phi)f_2(\phi')-\sin(\phi)f_1(\phi')\right]\Big|_{\phi_1}^{\phi_2} \tag{16}$$

Combining equations (7), (12) and (16) we obtain an expression for the magnetic vector potential:

$$\begin{aligned}\boldsymbol{A}(\rho,\phi,z) = \frac{\mu_0 I}{4\pi\rho}\{&-[\cos(\phi)f_1(\phi')+\sin(\phi)f_2(\phi')]\boldsymbol{e}_x\\ &+[\cos(\phi)f_2(\phi')-\sin(\phi)f_1(\phi')]\boldsymbol{e}_y\}\Big|_{\phi'=\phi_1}^{\phi_2}\end{aligned} \tag{17}$$

We now write the vector in (17) using its cylindrical components:

$$\boldsymbol{A}(\rho,\phi,z) = \frac{\mu_0 I}{4\pi\rho}\left[-f_1(\phi')\boldsymbol{e}_\rho + f_2(\phi')\boldsymbol{e}_\phi\right]\Big|_{\phi'=\phi_1}^{\phi_2} \tag{18}$$

IV. ANALYTICAL EXPRESSIONS FOR THE COMPONENTS OF THE MAGNETIC FIELD VECTOR

Let us express the magnetic field vector in equation (6) as:

$$\boldsymbol{B}(\rho,\phi,z)=\frac{\mu_0 I\rho'}{4\pi}(B_x\boldsymbol{e}_x+B_y\boldsymbol{e}_y+B_z\boldsymbol{e}_z) \tag{19}$$

where B_x, B_y and B_z are:

$$B_x=(z-z')\cdot\int_{\phi_1}^{\phi_2}\frac{\cos(\phi')d\phi'}{[\rho'^2+\rho^2+(z-z')^2-2\rho'\rho\cos(\phi'-\phi)]^{3/2}} \tag{20}$$

$$B_y=(z-z')\cdot\int_{\phi_1}^{\phi_2}\frac{\sin(\phi')d\phi'}{[\rho'^2+\rho^2+(z-z')^2-2\rho'\rho\cos(\phi'-\phi)]^{3/2}} \tag{21}$$

$$B_z=\int_{\phi_1}^{\phi_2}\frac{[\rho'-\rho\cos(\phi'-\phi)]d\phi'}{[\rho'^2+\rho^2+(z-z')^2-2\rho'\rho\cos(\phi'-\phi)]^{3/2}} \tag{22}$$

In this section we'll find an analytical solution using elliptic integrals for the integrals in equations (20) to (22). The integrals for B_x and B_y can be reduced to similar forms. The integral for B_z requires more work. For this reason, we'll make use of the following solved integrals:

$$\int_{\phi_1}^{\phi_2}\frac{\cos(\phi'-\phi)d\phi'}{[a-b\cos(\phi'-\phi)]^{3/2}}=\left\{\frac{2a}{b(a+b)^{3/2}}\Pi\left(\frac{\phi'-\phi-\pi}{2},\frac{2b}{a+b},\frac{2b}{a+b}\right)-\frac{2}{b\sqrt{a+b}}\mathrm{F}\left(\frac{\phi'-\phi-\pi}{2},\frac{2b}{a+b}\right)\right\}\Bigg|_{\phi_1}^{\phi_2} \tag{23}$$

$$\int_{\phi_1}^{\phi_2}\frac{\sin(\phi'-\phi)d\phi'}{[a-b\cos(\phi'-\phi)]^{3/2}}=-\frac{2}{b\sqrt{a-b\cos(\phi'-\phi)}}\Bigg|_{\phi_1}^{\phi_2} \tag{24}$$

$$\int_{\phi_1}^{\phi_2}\frac{[c-d\cos(\phi'-\phi)]d\phi'}{[a-b\cos(\phi'-\phi)]^{3/2}}=\left\{\frac{2(bc-ad)}{b(a+b)^{3/2}}\Pi\left(\frac{\phi'-\phi-\pi}{2},\frac{2b}{a+b},\frac{2b}{a+b}\right)+\frac{2d}{b\sqrt{a+b}}\mathrm{F}\left(\frac{\phi'-\phi-\pi}{2},\frac{2b}{a+b}\right)\right\}\Bigg|_{\phi_1}^{\phi_2} \tag{25}$$

The proofs of these equations are shown in the appendix of this article due to lengthy procedure. Here a, b, c and d are constants and F and Π are incomplete elliptic integrals of first and third kind, respectively. Let us focus first on the integral in equation (20). We start by doing some basic algebraic manipulations:

$$(z-z')\int_{\phi_1}^{\phi_2}\frac{\cos(\phi')d\phi'}{[\rho'^2+\rho^2+(z-z')^2-2\rho'\rho\cos(\phi'-\phi)]^{3/2}}$$
$$=(z-z')\int_{\phi_1}^{\phi_2}\frac{\cos(\phi'-\phi+\phi)d\phi'}{[\rho'^2+\rho^2+(z-z')^2-2\rho'\rho\cos(\phi'-\phi)]^{3/2}}$$

We now use the angle sum trigonometric identity:

$$(z-z')\int_{\phi_1}^{\phi_2}\frac{\cos(\phi'-\phi+\phi)d\phi'}{[\rho'^2+\rho^2+(z-z')^2-2\rho'\rho\cos(\phi'-\phi)]^{3/2}}$$
$$=(z-z')\int_{\phi_1}^{\phi_2}\frac{[\cos(\phi'-\phi)\cos(\phi)-\sin(\phi'-\phi)\sin(\phi)]d\phi'}{[\rho'^2+\rho^2+(z-z')^2-2\rho'\rho\cos(\phi'-\phi)]^{3/2}}$$

This integral has the form of the integrals described in formulas (23) and (24). We now apply the formulas with $a=\rho'^2+\rho^2+(z-z')^2$ and $b=2\rho'\rho$ to obtain:

$$B_x=\frac{(z-z')}{\rho'\rho}[\cos(\phi)f_4(\phi')+\sin(\phi)f_3(\phi')]\Bigg|_{\phi_1}^{\phi_2} \tag{26}$$

The functions f_3 and f_4 are used to reduce the length of the expressions and are useful for computational purposes. These functions are defined as:

$$f_3(\phi')=\frac{1}{\sqrt{\rho'^2+\rho^2+(z-z')^2-2\rho'\rho\cos(\phi'-\phi)}} \tag{27}$$

$$f_4(\phi')=\frac{\rho'^2+\rho^2+(z-z')^2}{[(\rho'+\rho)^2+(z-z')^2]^{3/2}}\Pi\left(\frac{\phi'-\phi-\pi}{2},m,m\right)-\frac{1}{\sqrt{(\rho'+\rho)^2+(z-z')^2}}\mathrm{F}\left(\frac{\phi'-\phi-\pi}{2},m\right) \tag{28}$$

Here, the parameter m is defined as:

$$m=\frac{4\rho'\rho}{(\rho'+\rho)^2+(z-z')^2} \tag{29}$$

The parameter m will take values between 0 and 1 for real positive values of ρ', ρ, z' and z. Now we focus on the integral in equation (21). Using a similar procedure and equations (27) and (28) we obtain:

$$B_y=\frac{(z-z')}{\rho'\rho}[-\cos(\phi)f_3(\phi')+\sin(\phi)f_4(\phi')]\Bigg|_{\phi_1}^{\phi_2} \tag{30}$$

We now apply the formula in equation (25) with $a=\rho'^2+\rho^2+(z-z')^2$, $b=2\rho'\rho$, $c=\rho'$ and $d=\rho$ to solve the integral in equation (22) to obtain:

$$B_z=\frac{f_5(\phi')}{\rho'} \tag{31}$$

where f_5 is defined as:

$$f_5(\phi')=-\frac{\rho^2-\rho'^2+(z-z')^2}{[(\rho'+\rho)^2+(z-z')^2]^{3/2}}\Pi\left(\frac{\phi'-\phi-\pi}{2},m,m\right)+\frac{1}{\sqrt{(\rho'+\rho)^2+(z-z')^2}}\mathrm{F}\left(\frac{\phi'-\phi-\pi}{2},m\right) \tag{32}$$

The parameter m is given by equation (29). With these results we can write an expression for the magnetic field vector in Cartesian coordinates:

$$\boldsymbol{B}(\rho,\phi,z)=\frac{\mu_0 I}{4\pi}\cdot\left\{\frac{(z-z')}{\rho}[\cos(\phi)f_4(\phi')+\sin(\phi)f_3(\phi')]\boldsymbol{e}_x\right.$$

$$+\frac{(z-z')}{\rho}[-\cos(\phi)f_3(\phi')+\sin(\phi)f_4(\phi')]\boldsymbol{e}_y$$
$$+f_5(\phi')\boldsymbol{e}_z\Big\}\Big|_{\phi'=\phi_1}^{\phi_2} \tag{33}$$

We now write the vector in (33) using its cylindrical components:

$$\boldsymbol{B}(\rho,\phi,z)=\frac{\mu_0 I}{4\pi}\Big[\frac{(z-z')}{\rho}f_4(\phi')\boldsymbol{e}_\rho$$
$$-\frac{(z-z')}{\rho}f_3(\phi')\boldsymbol{e}_\phi+f_5(\phi')\boldsymbol{e}_z\Big]\Big|_{\phi'=\phi_1}^{\phi_2} \tag{34}$$

Gauss' Magnetic Law $\nabla\cdot\boldsymbol{B}=0$ holds for expression (34) which provides a degree of validation.

V. SPECIAL CASE: CIRCULAR LOOP CARRYING A DIRECT CURRENT

A way to provide a degree of validation to the expression found in (34) is to study the case of a full circular loop. We start by recalling some elliptic integral properties [22]:

$$\mathrm{F}\left(\frac{\pi}{2},m\right)=\mathrm{K}(m)\quad \mathrm{E}\left(\frac{\pi}{2},m\right)=\mathrm{E}(m)$$
$$\Pi\left(\frac{\pi}{2},m,m\right)=\frac{\mathrm{E}(m)}{1-m}\quad \mathrm{F}\left(-\frac{\pi}{2},m\right)=-\mathrm{K}(m)$$
$$\mathrm{E}\left(-\frac{\pi}{2},m\right)=-\mathrm{E}(m)$$

Here $\mathrm{K}(m)$ and $\mathrm{E}(m)$ are complete elliptic integrals of the first and second kind, respectively. When evaluated at $\pi/2$, the incomplete elliptic integrals can be reduced to complete elliptic integrals as shown. Consider a circular loop of radius ρ' that goes from $\phi_1=0$ to $\phi_2=2\pi$. Due to the symmetry of the magnetic field, we can compute the magnetic field at a point located at $\phi=0$. Evaluating the expressions in (18) and (34) we obtain:

$$\boldsymbol{A}(\rho,\phi,z)=\frac{\mu_0 I}{2\pi\rho}\Big[\frac{\rho'^2+\rho^2+(z-z')^2}{\sqrt{(\rho'+\rho)^2+(z-z')^2}}\cdot\mathrm{K}(m)$$
$$-\sqrt{(\rho'+\rho)^2+(z-z')^2}\cdot\mathrm{E}(m)\Big]\boldsymbol{e}_\phi \tag{35}$$

$$\boldsymbol{B}(\rho,\phi,z)=\frac{\mu_0 I}{2\pi\sqrt{(\rho'+\rho)^2+(z-z')^2}}\Big\{\frac{(z-z')}{\rho}$$
$$\cdot\Big[\frac{\rho'^2+\rho^2+(z-z')^2}{(\rho-\rho')^2+(z-z')^2}\mathrm{E}(m)-\mathrm{K}(m)\Big]\boldsymbol{e}_\rho$$
$$-\Big[\frac{\rho^2-\rho'^2+(z-z')^2}{(\rho-\rho')^2+(z-z')^2}\mathrm{E}(m)-\mathrm{K}(m)\Big]\boldsymbol{e}_z\Big\} \tag{36}$$

These expressions match those expressions found in [14]. We can also examine the limiting case when $\rho\to 0$ to obtain a well-known expression:

$$B_\rho\to 0\quad B_z\to\frac{\mu_0\rho'^2 I}{2\left[\rho'^2+(z-z')^2\right]^{3/2}}$$

TABLE 1. Magnetic field components values generated by a circular loop of radius $\rho'=0.1$m. The loop is located at $z'=0$. The test points are located at $(0.05,\phi,0.1)$ where ϕ is varied. $k=\mu_0 I/4\pi$.

ρ(m)	ϕ(rads)	z(m)	$B_x/k(\mathrm{m}^{-1})$	$B_y/k(\mathrm{m}^{-1})$	$B_z/k(\mathrm{m}^{-1})$
0.05	0	0.1	7.8879	0.0000	18.9546
0.05	$\pi/3$	0.1	3.9439	6.8311	18.9546
0.05	$2\pi/3$	0.1	-3.9439	6.8311	18.9546
0.05	π	0.1	-7.8879	0.0000	18.9546
0.05	$4\pi/3$	0.1	-3.9439	-6.8311	18.9546
0.05	$5\pi/3$	0.1	3.9439	-6.8311	18.9546

TABLE 2. Magnetic field components values generated by a circular loop of radius $\rho'=0.1$m. The loop is located at $z'=0$. The test points are located at $(\rho,\phi,z)=(0.15,\phi,0.1)$ where ϕ is varied. $k=\mu_0 I/4\pi$.

ρ(m)	ϕ(rads)	z(m)	$B_x/k(\mathrm{m}^{-1})$	$B_y/k(\mathrm{m}^{-1})$	$B_z/k(\mathrm{m}^{-1})$
0.15	0	0.1	8.0088	0.0000	1.7668
0.15	$\pi/3$	0.1	4.0044	6.9358	1.7668
0.15	$2\pi/3$	0.1	-4.0044	6.9358	1.7668
0.15	π	0.1	-8.0088	0.0000	1.7668
0.15	$4\pi/3$	0.1	-4.0044	-6.9358	1.7668
0.15	$5\pi/3$	0.1	4.0044	-6.9358	1.7668

For a numerical example, consider a circular loop of radius $\rho'=0.1$ m placed at $z'=0$ m. We take points inside the loop at $\rho=0.05$ m and $z=0.1$ m. We vary ϕ to obtain the magnetic field at different points inside. The results are shown in Table 1.

We now take points outside of the radius of the loop at $\rho=0.15$ m and $z=0.1$ m. We vary ϕ to obtain the magnetic field at different points outside the loop. The results are shown in Table 2.

As a graphical validation, we plot the magnetic vector potential and the magnetic field (in 2D and in 3D) for this example. See Figure 2.

VI. STUDY CASES

Case Study 1: Consider a circular arc filament of radius $\rho'=0.1$ m placed at $z'=0$ m. The arc loop for this case study goes from $\phi_1=0$ rads to $\phi_2=\pi/2$ rads. In Table 3 values for the magnetic field components generated by this loop are shown for points at $(\rho,\phi,z)=(0.05,\phi,0.25)$. In Table 4 values for the magnetic field components generated by this loop are shown for points at $(\rho,\phi,z)=(0.15,\phi,0.25)$. The magnetic vector potential plot and magnetic field vector plots for this loop are shown in Figure 3.

Case Study 2: Consider a circular arc filament of radius $\rho'=0.5$ m placed at $z'=0$ m. The arc loop for this case study goes from $\phi_1=0$ rads to $\phi_2=\pi$ rads. In Table 5 values for the magnetic field components generated by this loop are shown for points at $(\rho,\phi,z)=(0.25,\phi,0.17)$. In Table 6 values for the magnetic field components generated by this loop are shown for points at $(\rho,\phi,z)=(0.75,\phi,0.17)$. The magnetic vector potential plot and magnetic field vector plots for this loop are shown in Figure 4.

Case Study 3: Consider a circular arc filament of radius $\rho'=0.275$ m placed at $z'=0$ m. The arc loop for

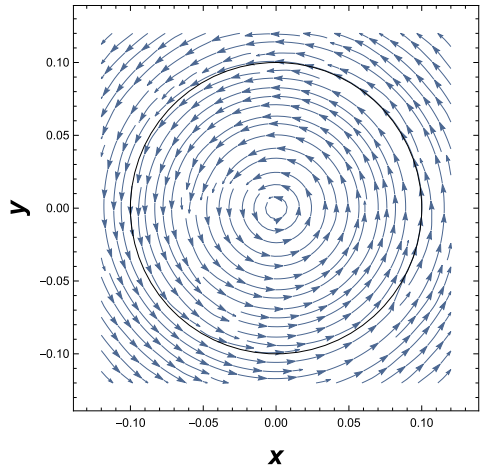

(a)

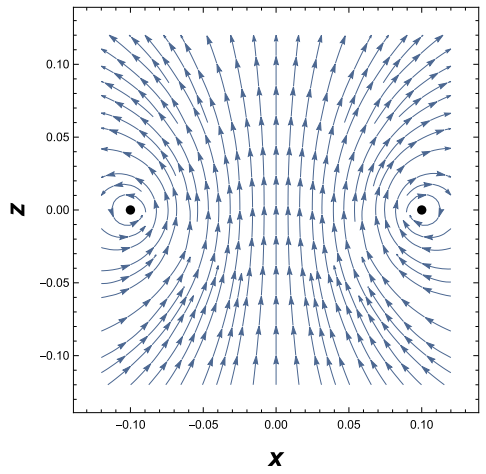

(b)

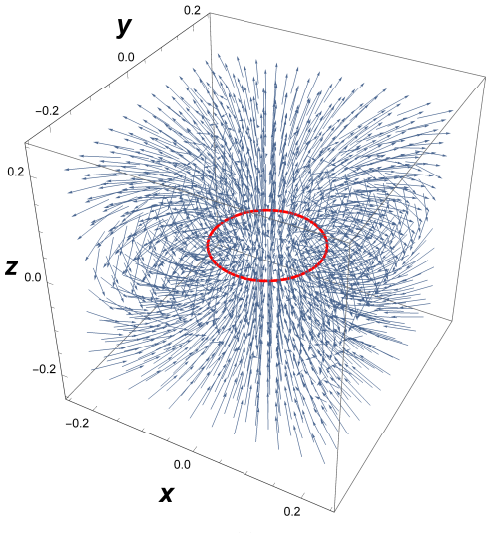

(c)

FIGURE 2. Special Case Study. Magnetic vector potential and magnetic field vector plots generated by a circular loop of radius $\rho' = 0.1$ m located at $z' = 0$ m. (a) Magnetic vector potential streamline plot as seen from the xy-plane at $z = 0$. (b) Magnetic field vector streamline plot as seen from the xz-plane at $y = 0$. (c) Magnetic field 3D vector plot. For this plot, the loop is shown and the vector arrows are all scaled to the same size.

TABLE 3. Magnetic field components values generated by a circular arc filament of radius $\rho' = 0.1$m. The loop is located at $z' = 0$ m. The test points are located at $(\rho, \phi, z) = (0.05, \phi, 0.25)$ where ϕ is varied. $k = \mu_0 I/4\pi$.

ρ(m)	ϕ(rads)	z(m)	$B_x/k(\mathrm{m}^{-1})$	$B_y/k(\mathrm{m}^{-1})$	$B_z/k(\mathrm{m}^{-1})$
0.05	0	0.25	1.4397	1.3542	0.5889
0.05	$\pi/3$	0.25	1.4513	1.4850	0.5185
0.05	$2\pi/3$	0.25	1.2324	1.3352	0.6986
0.05	π	0.25	1.0497	1.1076	0.8886
0.05	$4\pi/3$	0.25	1.0413	1.0216	0.9301
0.05	$5\pi/3$	0.25	1.2124	1.1233	0.8077

TABLE 4. Magnetic field components values generated by a circular arc filament of radius $\rho' = 0.1$m. The loop is located at $z' = 0$ m. The test points are located at $(\rho, \phi, z) = (0.15, \phi, 0.25)$ where ϕ is varied. $k = \mu_0 I/4\pi$.

ρ(m)	ϕ(rads)	z(m)	$B_x/k(\mathrm{m}^{-1})$	$B_y/k(\mathrm{m}^{-1})$	$B_z/k(\mathrm{m}^{-1})$
0.15	0	0.25	1.3289	1.1298	-0.0261
0.15	$\pi/3$	0.25	1.3538	1.4419	-0.2814
0.15	$2\pi/3$	0.25	0.8932	1.0905	0.3257
0.15	π	0.25	0.6164	0.6933	0.7827
0.15	$4\pi/3$	0.25	0.6048	0.5807	0.8568
0.15	$5\pi/3$	0.25	0.8568	0.7176	0.6122

TABLE 5. Magnetic field components values generated by a circular arc filament of radius $\rho' = 0.5$m. The loop is located at $z' = 0$ m. The test points are located at $(\rho, \phi, z) = (0.25, \phi, 0.17)$ where ϕ is varied. $k = \mu_0 I/4\pi$.

ρ(m)	ϕ(rads)	z(m)	$B_x/k(\mathrm{m}^{-1})$	$B_y/k(\mathrm{m}^{-1})$	$B_z/k(\mathrm{m}^{-1})$
0.25	0	0.17	1.6871	1.3650	5.6761
0.25	$\pi/3$	0.17	1.4389	3.4244	8.1524
0.25	$2\pi/3$	0.17	-1.4389	3.4244	8.1524
0.25	pi	0.17	-1.6871	1.3650	5.6761
0.25	$4\pi/3$	0.17	-0.2483	0.5022	3.1998
0.25	$5\pi/3$	0.17	0.2483	0.5022	3.1998

TABLE 6. Magnetic field components values generated by a circular arc filament of radius $\rho' = 0.5$m. The loop is located at $z' = 0$ m. The test points are located at $(\rho, \phi, z) = (0.75, \phi, 0.17)$ where ϕ is varied. $k = \mu_0 I/4\pi$.

ρ(m)	ϕ(rads)	z(m)	$B_x/k(\mathrm{m}^{-1})$	$B_y/k(\mathrm{m}^{-1})$	$B_z/k(\mathrm{m}^{-1})$
0.75	0	0.17	1.2553	0.5701	-0.9084
0.75	$\pi/3$	0.17	1.1789	2.2947	-2.8001
0.75	$2\pi/3$	0.17	-1.1789	2.2947	-2.8001
0.75	π	0.17	-1.2553	0.5701	-0.9084
0.75	$4\pi/3$	0.17	-0.0763	0.1205	0.9833
0.75	$5\pi/3$	0.17	0.0763	0.1205	0.9833

this case study goes from $\phi_1 = 0$ rads to $\phi_2 = 3\pi/2$ rads. In Table 7 values for the magnetic field components generated by this loop are shown for points at $(\rho, \phi, z) = (0.1375, \phi, -0.2)$. In Table 8 values for the magnetic field components generated by this loop are shown for points at $(\rho, \phi, z) = (0.4125, \phi, -0.2)$. The magnetic vector potential plot and magnetic field vector plots for this loop are shown in Figure 5.

Case Study 4: Consider a circular arc filament of radius $\rho' = 0.2$ m placed at $z' = 0$ m. The arc loop for this

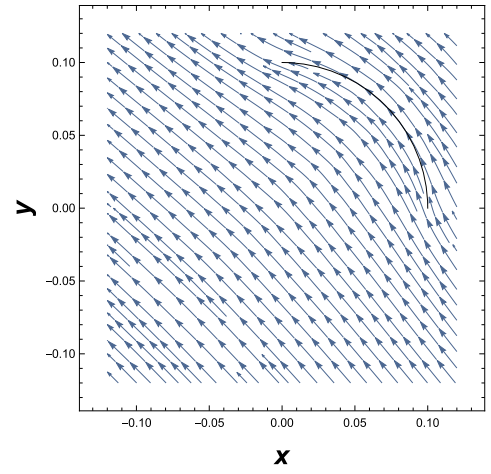

(a)

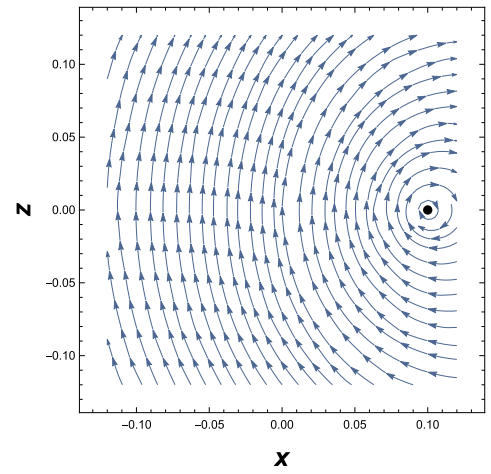

(b)

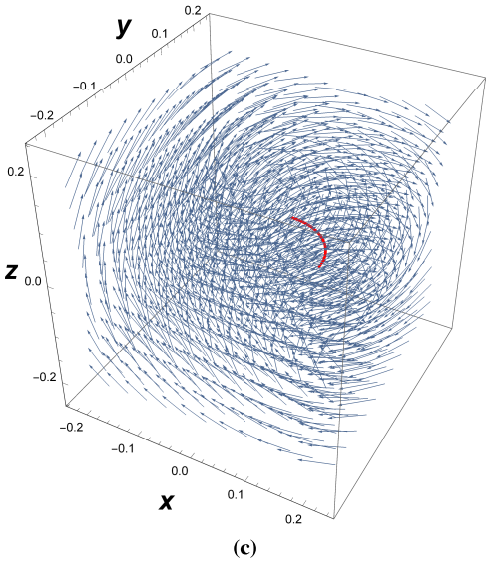

(c)

FIGURE 3. **Case Study 1.** Magnetic vector potential and magnetic field vector plots generated by a circular arc filament of radius $\rho' = 0.1$ m located at $z' = 0$ m. (a) Magnetic vector potential streamline plot as seen from the plane $z = 0$. (b) Magnetic field vector streamline plot as seen from the plane $y = 0$. (c) Magnetic field 3D vector plot. For this plot, the loop is shown and the vector arrows are all scaled to the same size.

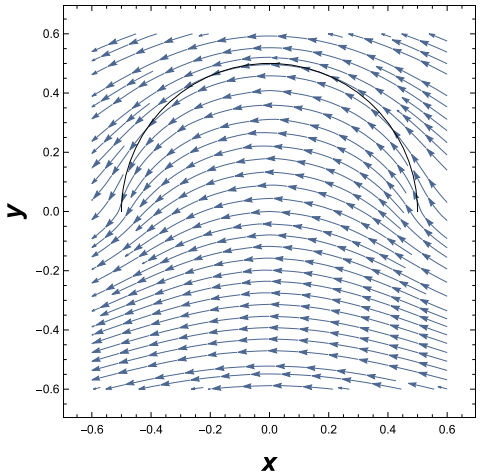

(a)

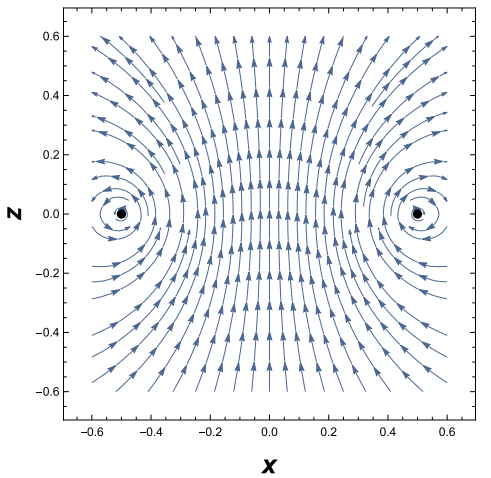

(b)

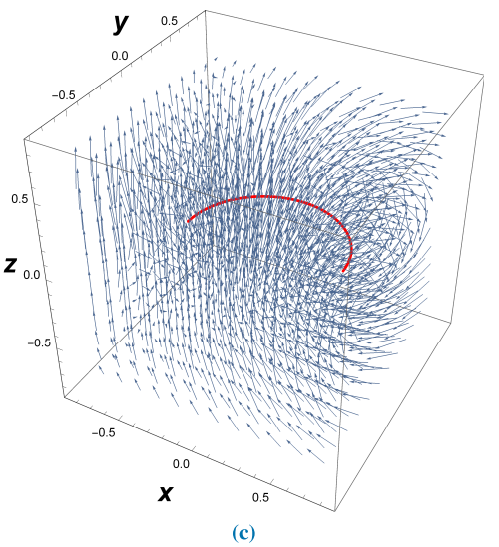

(c)

FIGURE 4. **Case Study 2.** Magnetic vector potential and magnetic field vector plots generated by a circular arc filament of radius $\rho' = 0.5$ m located at $z' = 0$ m. (a) Magnetic vector potential streamline plot as seen from the plane $z = 0$. (b) Magnetic field vector streamline plot as seen from the plane $y = 0$. (c) Magnetic field 3D vector plot. For this plot, the loop is shown and the vector arrows are all scaled to the same size.

TABLE 7. Magnetic field components values generated by a circular arc filament of radius $\rho' = 0.275$ m. The loop is located at $z' = 0$ m. The test points are located at $(\rho, \phi, z) = (0.1375, \phi, -0.2)$ where ϕ is varied. $k = \mu_0 I/4\pi$.

ρ(m)	ϕ(rads)	z(m)	$B_x/k(\mathrm{m}^{-1})$	$B_y/k(\mathrm{m}^{-1})$	$B_z/k(\mathrm{m}^{-1})$
0.1375	0	-0.2	-1.5765	-2.0274	7.3778
0.1375	$\pi/3$	-0.2	-1.0748	-4.7111	8.4193
0.1375	$2\pi/3$	-0.2	2.8646	-4.4587	8.8043
0.1375	π	-0.2	5.1170	-0.7928	8.6848
0.1375	$4\pi/3$	-0.2	3.4963	1.9916	7.9682
0.1375	$5\pi/3$	-0.2	0.7422	0.4321	6.9335

TABLE 8. Magnetic field components values generated by a circular arc filament of radius $\rho' = 0.275$ m. The loop is located at $z' = 0$ m. The test points are located at $(\rho, \phi, z) = (0.4125, \phi, -0.2)$ where ϕ is varied. $k = \mu_0 I/4\pi$.

ρ(m)	ϕ(rads)	z(m)	$B_x/k(\mathrm{m}^{-1})$	$B_y/k(\mathrm{m}^{-1})$	$B_z/k(\mathrm{m}^{-1})$
0.4125	0	-0.2	-1.7883	-1.0907	0.7619
0.4125	$\pi/3$	-0.2	-1.5715	-3.6613	-0.8644
0.4125	$2\pi/3$	-0.2	2.1379	-3.5647	-0.9193
0.4125	π	-0.2	4.1130	-0.2298	-0.9191
0.4125	$4\pi/3$	-0.2	2.4373	2.5114	-0.5036
0.4125	$5\pi/3$	-0.2	0.2454	0.4840	1.9728

TABLE 9. Magnetic field components values generated by a circular arc filament of radius $\rho' = 0.2$ m. The loop is located at $z' = 0$ m. The test points are located at $(\rho, \phi, z) = (0.1, \phi, -0.1)$ where ϕ is varied. $k = \mu_0 I/4\pi$.

ρ(m)	ϕ(rads)	z(m)	$B_x/k(\mathrm{m}^{-1})$	$B_y/k(\mathrm{m}^{-1})$	$B_z/k(\mathrm{m}^{-1})$
0.1	0	-0.1	-1.2168	-3.0291	6.4401
0.1	$\pi/3$	-0.1	-2.0629	-7.9674	10.9171
0.1	$2\pi/3$	-0.1	2.0629	-7.9674	10.9171
0.1	π	-0.1	1.2168	-3.0291	6.4401
0.1	$4\pi/3$	-0.1	0.1886	-1.3372	4.3720
0.1	$5\pi/3$	-0.1	-0.1886	-1.3372	4.3720

TABLE 10. Magnetic field components values generated by a circular arc filament of radius $\rho' = 0.2$ m. The loop is located at $z' = 0$ m. The test points are located at $(\rho, \phi, z) = (0.3, \phi, -0.1)$ where ϕ is varied. $k = \mu_0 I/4\pi$.

ρ(m)	ϕ(rads)	z(m)	$B_x/k(\mathrm{m}^{-1})$	$B_y/k(\mathrm{m}^{-1})$	$B_z/k(\mathrm{m}^{-1})$
0.3	0	-0.1	-0.6241	-1.0800	0.9788
0.3	$\pi/3$	-0.1	-2.2691	-5.6584	-4.7570
0.3	$2\pi/3$	-0.1	2.2691	-5.6584	-4.7570
0.3	π	-0.1	0.6241	-1.0800	0.9788
0.3	$4\pi/3$	-0.1	0.0572	-0.3328	1.6069
0.3	$5\pi/3$	-0.1	-0.0572	-0.3328	1.6069

case study goes from $\phi_1 = \pi/6$ rads to $\phi_2 = 5\pi/6$ rads. In Table 9 values for the magnetic field components generated by this loop are shown for points at $(\rho, \phi, z) = (0.1, \phi, -0.1)$. In Table 10 values for the magnetic field components generated by this loop are shown for points at $(\rho, \phi, z) = (0.3, \phi, -0.1)$. The magnetic vector potential plot and magnetic field vector plots for this loop are shown in Figure 6.

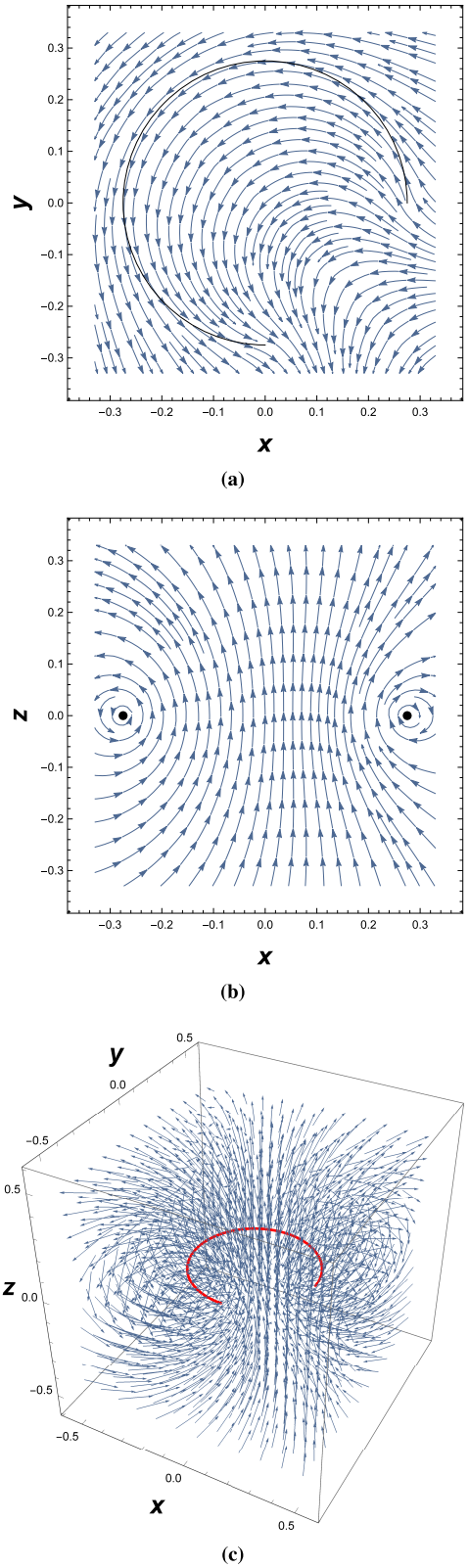

FIGURE 5. Case Study 3. Magnetic vector potential and magnetic field vector plots generated by a circular arc filament of radius $\rho' = 0.275$ m located at $z' = 0$ m. (a) Magnetic vector potential streamline plot as seen from the plane $z = 0$. (b) Magnetic field vector streamline plot as seen from the plane $y = 0$. (c) Magnetic field 3D vector plot. For this plot, the loop is shown and the vector arrows are all scaled to the same size.

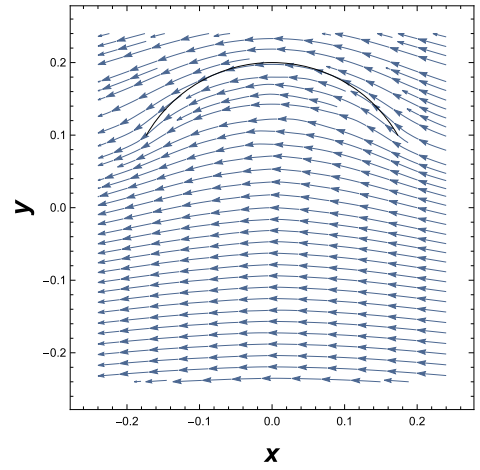

(a)

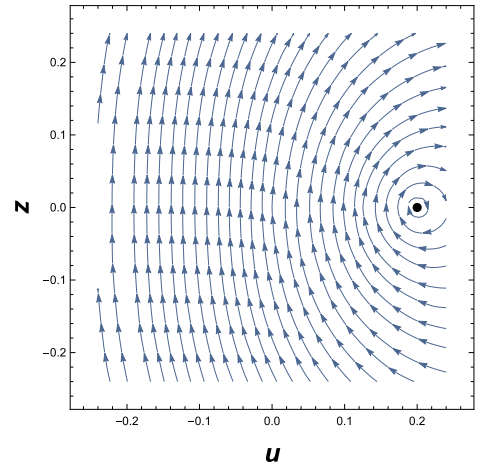

(b)

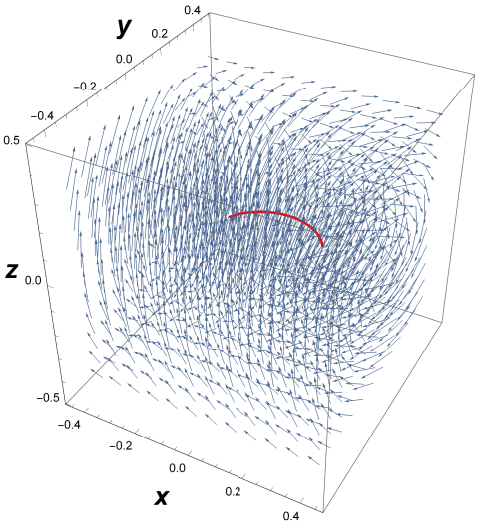

(c)

FIGURE 6. **Case Study 4. Magnetic vector potential and magnetic field vector plots generated by a circular arc filament of radius $\rho' = 0.2$ m located at $z' = 0$ m. (a) Magnetic vector potential streamline plot as seen from the plane $z = 0$. (b) Magnetic field vector streamline plot as seen from the plane $(\sqrt{3}/3)x - y = 0$. (c) Magnetic field 3D vector plot. For this plot, the loop is shown and the vector arrows are all scaled to the same size.**

VII. NUMERICAL VALIDATION OF THE ANALYTICAL EXPRESSIONS

Another way to validate the derived expressions is to compare the results of the formulas with numerical results obtained from a numerical method applied directly to the integrals in equations (5) and (6). In this section, we use Wolfram Mathematica's Global Adaptive Strategy for computational integration and then compare the numerical results from this method with the ones obtained from the derived formulas. The evaluation of the elliptic integrals is also done with Mathematica. Let us consider the following case study.

Case Study: Consider a circular arc filament of radius $\rho' = 0.125$ m placed at $z' = 0$ m. The arc loop for this case study goes from $\phi_1 = 5\pi/36$ rads to $\phi_2 = 7\pi/4$ rads. The components values for the magnetic vector potential are calculated using, both, numerical integration (A_{i-x} and A_{i-y}) and elliptic integrals formulas (A_x and A_y). The results of these calculations are shown in Table 11, at test points with coordinates $(\rho, \phi, z) = (0.1875, \phi, 0.15)$.

TABLE 11. **Magnetic vector potential components values generated by a circular arc filament of radius $\rho' = 0.125$ m. The loop is located at $z' = 0$ m. The test points are located at $(\rho, \phi, z) = (0.1875, \phi, 0.15)$ where ϕ is varied. The values are computed using numerical integration and elliptic integrals formulas. $k = \mu_0 I/4\pi$.**

ϕ(rads)	A_{i-x}/k	A_{i-y}/k	A_x/k	A_y/k
0	-0.1325	-0.2368	-0.1325	-0.2368
$\pi/3$	-0.5861	-0.3113	-0.5861	-0.3113
$2\pi/3$	-0.5775	-0.7410	-0.5775	-0.7410
π	-0.0747	-1.0008	-0.0747	-1.0008
$4\pi/3$	0.4091	-0.7714	0.4091	-0.7714
$5\pi/3$	0.3545	-0.3847	0.3545	-0.3847

The components values for the magnetic vector field are calculated using, both, numerical integration (B_{i-x}, B_{i-y} and B_{i-z}) and elliptic integrals formulas (B_x, B_y and B_z). The results of these calculations are shown in Table 12, at test points with coordinates $(\rho, \phi, z) = (0.1875, \phi, 0.15)$.

TABLE 12. **Magnetic field components values generated by a circular arc filament of radius $\rho' = 0.125$ m. The loop is located at $z' = 0$ m. The test points are located at $(\rho, \phi, z) = (0.1875, \phi, 0.15)$ where ϕ is varied. $k = \mu_0 I/4\pi$.**

ϕ(rads)	B_{i-x}	B_{i-y}	B_{i-z}	B_x	B_y	B_z
0	0.7899	0.5653	3.3688	0.7899	0.5653	3.3688
$\pi/3$	0.7699	4.4255	1.3170	0.7699	4.4255	1.3170
$2\pi/3$	-3.2014	4.4394	0.7225	-3.2014	4.4394	0.7225
π	-5.5731	0.1010	0.6899	-5.5731	0.1010	0.6899
$4\pi/3$	-3.3586	-4.1347	0.7910	-3.3586	-4.1347	0.7910
$5\pi/3$	0.0436	-3.5543	1.9630	0.0436	-3.5543	1.9630

Although it may seem that there is no difference between values computed through the numerical method and the values computed through the elliptic integrals formulas, there does exist a difference in the truncated decimals. The differences are presented in Table 13. This differences are calculated by taking the absolute value of the difference between

TABLE 13. Magnetic field components values generated by a circular arc filament of radius $\rho' = 0.125$ m. The loop is located at $z' = 0$ m. The test points are located at $(\rho, \phi, z) = (0.1875, \phi, 0.15)$ where ϕ is varied. $k = \mu_0 I/4\pi$.

ϕ(rads)	ϵ_{A_x}	ϵ_{A_y}	ϵ_{B_x}	ϵ_{B_y}	ϵ_{B_z}
0	1.3807E-12	5.4970E-13	9.9956E-12	1.6461E-11	5.1026E-13
$\pi/3$	6.4704E-10	2.7411E-10	4.7962E-14	4.2598E-09	5.1958E-14
$2\pi/3$	1.8531E-08	4.3681E-09	1.7764E-15	9.4147E-13	3.0087E-14
π	1.4333E-13	1.6891E-09	0.0000E+00	4.0246E-16	7.9936E-15
$4\pi/3$	1.0763E-08	2.2173E-09	1.3323E-15	1.7764E-15	5.7732E-15
$5\pi/3$	4.7129E-11	3.5363E-11	2.5327E-15	6.0988E-09	1.3731E-12

the numerical method value and the proposed elliptic integrals formulas.

From this we conclude that the elliptic integrals formulas can be as reliable as a known numerical method. It must be noted that these differences will be different if another numerical method is used or if another elliptic integrals evaluation method is used.

VIII. CONCLUSION

In this paper, we could show that we can break the seemingly complex magnetic field integrals generated by circular arc loop carrying a direct current down into integrals that have a similar method of solution. Through the use of recurrence formulas for integrals of elliptic functions, we were able to find analytical solutions to these integrals in terms of the well-known incomplete and complete elliptic integrals. We find the numerical methods for evaluating elliptic integrals in the literature. In computing systems like Wolfram Mathematica and programming languages like MATLAB [23], these methods are already programmed and ready to use. These elliptic integral methods have results as accurate as classical numerical methods and the mathematical properties of the expressions for magnetic vector potential and magnetic field vector can be studied based on the mathematical properties of the elliptic integrals. The simple algebraic structure of the expressions makes possible to program the expressions for engineering problems like wireless power systems. This simple structure makes easy to use these expressions to derive more complex formulas such as magnetic coupling, which is planned for future research.

In conclusion, we were able to derive formulas for the magnetic vector potential and magnetic field vector using elliptic integrals. We have validated the expressions through the reduction of the general formulas to more specific special cases and the self-consistency of the equations using Gauss's magnetic law. The methods developed in this paper can be used to derive similar formulas for higher dimensional magnetic field problems. The expressions can be easily programmed in any scientific programming language and can be used to derive expressions for more complex problems such as those regarding magnetic coupling between the coils of a wireless power transfer system. Finally, we provided several numerical examples of unstudied cases in which we plot the magnetic vector potential and the magnetic field to examine the shape of the fields generated by these interesting geometries.

APPENDIX A INTEGRAL FORMULAS

It is important to specify the definitions of incomplete elliptic integrals used in this article. The incomplete elliptic integral of the first kind is defined as:

$$\mathrm{F}(\phi, m) = \int_0^{\phi} \frac{1}{\sqrt{1 - m\sin^2(\theta)}} d\theta \tag{A.1}$$

The incomplete elliptic integral of the second kind is defined as:

$$\mathrm{E}(\phi, m) = \int_0^{\phi} \sqrt{1 - m\sin^2(\theta)} d\theta \tag{A.2}$$

The incomplete elliptic integral of the third kind is defined as:

$$\Pi(\phi, m, n) = \int_0^{\phi} \frac{d\theta}{[1 + n\sin^2(\theta)]\sqrt{1 - m\sin^2(\theta)}} \tag{A.3}$$

Here we'll derive the integral formulas required to solve for the expression of the magnetic field generated by a circular arc loop. The proofs are presented in a didactic, easy to follow way. In most of these integrals, the challenge lies in the angular difference $\phi' - \phi$ as it can't be easily integrated and it should be reduced to a single angle by using the trick substitution $2\psi + \pi = \phi' - \phi$. Most of the integrals can be reduced to known forms found in [22].

Theorem 1: Let a, b and ϕ be real constants. For $a > 0$, $b > 0$ and $b < a$ we have the following equation:

$$\int \frac{\sin(\phi' - \phi)}{\sqrt{a - b\cos(\phi' - \phi)}} d\phi' = \frac{2\sqrt{a - b\cos(\phi' - \phi)}}{b} + C \tag{A.4}$$

where C is an arbitrary constant.

Proof: We start by doing a simple substitution where $u = \cos(\phi' - \phi)$ and $du = -\sin(\phi' - \phi)d\phi'$:

$$\int \frac{\sin(\phi' - \phi)}{\sqrt{a - b\cos(\phi' - \phi)}} d\phi' = -\int \frac{du}{\sqrt{a - bu}}$$

Integrating the function of u we obtain:

$$-\int \frac{du}{\sqrt{a - bu}} du = \frac{2\sqrt{a - bu}}{b} + C$$

Now we change back to the original variables:

$$\int \frac{\sin(\phi' - \phi)}{\sqrt{a - b\cos(\phi' - \phi)}} d\phi' = \frac{2\sqrt{a - b\cos(\phi' - \phi)}}{b} + C$$

Theorem 2: Let a, b and ϕ be real constants. For $a > 0$, $b > 0$ and $b < a$ we have the following equation:

$$\int \frac{\cos(\phi' - \phi)}{\sqrt{a - b\cos(\phi' - \phi)}} d\phi' = \frac{2a}{b\sqrt{a + b}} \mathrm{F}\left(\frac{\phi' - \phi - \pi}{2}, \frac{2b}{a + b}\right)$$

$$-\frac{2\sqrt{a+b}}{b}\mathrm{E}\left(\frac{\phi'-\phi-\pi}{2},\frac{2b}{a+b}\right)+C \qquad (A.5)$$

where C is an arbitrary constant and F *and* E *are incomplete elliptic integrals of the first and second kind, respectively.*

Proof: We start by using the simple substitution $2\psi + \pi = \phi' - \phi$ and $2d\psi = d\phi'$:

$$\int \frac{\cos(\phi'-\phi)}{\sqrt{a-b\cos(\phi'-\phi)}}d\phi' = 2\int \frac{\cos(2\psi+\pi)}{\sqrt{a-b\cos(2\psi+\pi)}}d\psi$$

We now apply the trigonometric property of the cosine $\cos(2\psi+\pi) = -\cos(2\psi)$:

$$2\int \frac{\cos(2\psi+\pi)}{\sqrt{a-b\cos(2\psi+\pi)}}d\psi = -2\int \frac{\cos(2\psi)}{\sqrt{a+b\cos(2\psi)}}d\psi$$

We apply the double angle trigonometric identity and we factor the expression inside the square root in the denominator:

$$-2\int \frac{\cos(2\psi)}{\sqrt{a+b\cos(2\psi)}}d\psi = -\frac{2}{\sqrt{b}}\int \frac{1-2\sin^2(\psi)}{\sqrt{\frac{a}{b}+1-2\sin^2(\psi)}}d\psi$$

Factoring the expression inside the square root in the denominator once more:

$$-\frac{2}{\sqrt{b}}\int \frac{1-2\sin^2(\psi)}{\sqrt{\frac{a}{b}+1-2\sin^2(\psi)}}d\psi = -\frac{2}{\sqrt{a+b}}\int \frac{1-2\sin^2(\psi)}{\sqrt{1-m\sin^2(\psi)}}d\psi$$

Here $m = 2b/(a+b)$. By using Jacobi elliptic functions to make a change of variables in the integral we are able to reduce the integral to a known form. Using the Jacobi elliptic functions, we make a substitution where $\mathrm{sn}(u,m) = \sin(\psi)$, $\mathrm{dn}(u,m) = \sqrt{1-m\sin^2(\psi)}$ and $d\psi/du = \mathrm{dn}(u,m) = \sqrt{1-m\sin^2(\psi)}$. Here $\mathrm{am}(u) = \psi$ and $u = \mathrm{F}(\psi, m)$. We now substitute:

$$-\frac{2}{\sqrt{a+b}}\int \frac{1-2\sin^2(\psi)}{\sqrt{1-m\sin^2(\psi)}}d\psi = -\frac{2}{\sqrt{a+b}}\int \left[1-2\mathrm{sn}^2(u,m)\right]du$$

Applying the formulas (310.00) and (310.02) found in [22] we find the following expression:

$$-\frac{2}{\sqrt{a+b}}\int \left[1-2\mathrm{sn}^2(u,m)\right]du = -\frac{2}{m\sqrt{a+b}}\left[(m-2)\mathrm{F}(\psi,m)+2\mathrm{E}(\psi,m)\right]+C$$

where C is an arbitrary constant and F and E are incomplete elliptic integrals of the first and second kind, respectively. By changing variables to the original variables and doing some algebra with the help of Wolfram Mathematica, we obtain the final expression:

$$\int \frac{\cos(\phi'-\phi)}{\sqrt{a-b\cos(\phi'-\phi)}}d\phi' = \frac{2a}{b\sqrt{a+b}}\mathrm{F}\left(\frac{\phi'-\phi-\pi}{2},\frac{2b}{a+b}\right) - \frac{2\sqrt{a+b}}{b}\mathrm{E}\left(\frac{\phi'-\phi-\pi}{2},\frac{2b}{a+b}\right)+C$$

Theorem 3: Let a, b and ϕ be real constants. For $a > 0$, $b > 0$ and $b < a$ we have the following equation:

$$\int \frac{\sin(\phi'-\phi)}{[a-b\cos(\phi'-\phi)]^{3/2}}d\phi' = -\frac{2}{b\sqrt{a-b\cos(\phi'-\phi)}}+C \qquad (A.6)$$

where C is an arbitrary constant.

Proof: We start by doing a simple substitution where $u = \cos(\phi'-\phi)$ and $du = -\sin(\phi'-\phi)d\phi'$:

$$\int \frac{\sin(\phi'-\phi)}{[a-b\cos(\phi'-\phi)]^{3/2}}d\phi' = -\int \frac{du}{[a-bu]^{3/2}}$$

Integrating the function of u we obtain:

$$-\int \frac{du}{[a-bu]^{3/2}} = -\frac{2}{b\sqrt{a-bu}}+C$$

Now we change back to the original variables:

$$\int \frac{\sin(\phi'-\phi)}{[a-b\cos(\phi'-\phi)]^{3/2}}d\phi' = -\frac{2}{b\sqrt{a-b\cos(\phi'-\phi)}}+C$$

Theorem 4: Let a, b and ϕ be real constants. For $a > 0$, $b > 0$ and $b < a$ we have the following equation:

$$\int \frac{\cos(\phi'-\phi)}{[a-b\cos(\phi'-\phi)]^{3/2}}d\phi' = \frac{2a}{b(a+b)^{3/2}}\Pi\left(\frac{\phi'-\phi-\pi}{2},\frac{2b}{a+b},\frac{2b}{a+b}\right) - \frac{2}{b\sqrt{a+b}}\mathrm{F}\left(\frac{\phi'-\phi-\pi}{2},\frac{2b}{a+b}\right)+C \qquad (A.7)$$

where C is an arbitrary constant and F and Π are incomplete elliptic integrals of the first and third kind, respectively.

Proof: We start by using the simple substitution $2\psi + \pi = \phi' - \phi$ and $2d\psi = d\phi'$:

$$\int \frac{\cos(\phi'-\phi)}{[a-b\cos(\phi'-\phi)]^{3/2}}d\phi' = 2\int \frac{\cos(2\psi+\pi)}{[a-b\cos(2\psi+\pi)]^{3/2}}d\psi$$

We now apply the trigonometric property of the cosine $\cos(2\psi+\pi) = -\cos(2\psi)$:

$$2\int \frac{\cos(2\psi+\pi)}{[a-b\cos(2\psi+\pi)]^{3/2}}d\psi$$

$$= -2\int \frac{\cos(2\psi)}{[a+b\cos(2\psi)]^{3/2}}d\psi$$

We apply the double angle trigonometric identity and we factor the expression inside the root in the denominator:

$$-2\int \frac{\cos(2\psi)}{[a+b\cos(2\psi)]^{3/2}}d\psi = -\frac{2}{(b)^{3/2}}\int \frac{1-2\sin^2(\psi)}{\left[\frac{a}{b}+1-2\sin^2\psi\right]^{3/2}}d\psi$$

Factoring the expression inside the root in the denominator once more:

$$-\frac{2}{(b)^{3/2}}\int \frac{1-2\sin^2(\psi)}{\left[\frac{a}{b}+1-2\sin^2\psi\right]^{3/2}}d\psi = -\frac{2}{(a+b)^{3/2}}\int \frac{1-2\sin^2(\psi)}{\left[1-m\sin^2(\psi)\right]^{3/2}}d\psi$$

Here $m = 2b/(a+b)$. By using Jacobi elliptic functions to make a change of variables in the integral we are able to reduce the integral to a known form. Using the Jacobi elliptic functions, we make a substitution where $\mathrm{sn}(u,m) = \sin(\psi)$, $\mathrm{dn}(u,m) = \sqrt{1-m\sin^2(\psi)}$ and $d\psi/du = \mathrm{dn}(u,m) = \sqrt{1-m\sin^2(\psi)}$. Here $\mathrm{am}(u) = \psi$ and $u = \mathrm{F}(\psi,m)$. We now substitute:

$$-\frac{2}{(a+b)^{3/2}}\int \frac{1-2\sin^2(\psi)}{\left[1-m\sin^2(\psi)\right]^{3/2}}d\psi = -\frac{2}{(a+b)^{3/2}}\int \frac{1-2\mathrm{sn}^2(u,m)}{1-m\,\mathrm{sn}^2(u,m)}du$$

Applying the formula (340.01) found in [22] we find the following expression:

$$-\frac{2}{(a+b)^{3/2}}\int \frac{1-2\mathrm{sn}^2(u,m)}{1-m\,\mathrm{sn}^2(u,m)}du = -\frac{2}{m(a+b)^{3/2}}\left[(m-2)\Pi\left(\psi,m,m\right)+2\mathrm{F}\left(\psi,m\right)\right]+C$$

where C is an arbitrary constant and F and Π are incomplete elliptic integrals of the first and third kind, respectively. By changing variables to the original variables and doing some algebra with the help of Wolfram Mathematica, we obtain the final expression:

$$\int \frac{\cos(\phi'-\phi)}{[a-b\cos(\phi'-\phi)]^{3/2}}d\phi' = \frac{2a}{b(a+b)^{3/2}}\Pi\left(\frac{\phi'-\phi-\pi}{2},\frac{2b}{a+b},\frac{2b}{a+b}\right) - \frac{2}{b\sqrt{a+b}}\mathrm{F}\left(\frac{\phi'-\phi-\pi}{2},\frac{2b}{a+b}\right)+C$$

Theorem 5: Let a, b and ϕ be real constants. For $a > 0$, $b > 0$ and $b < a$ we have the following equation:

$$\int \frac{c-d\cos(\phi'-\phi)}{[a-b\cos(\phi'-\phi)]^{3/2}}d\phi' = \frac{2(bc-ad)}{b(a+b)^{3/2}}\Pi\left(\frac{\phi'-\phi-\pi}{2},\frac{2b}{a+b},\frac{2b}{a+b}\right) + \frac{2d}{b\sqrt{a+b}}\mathrm{F}\left(\frac{\phi'-\phi-\pi}{2},\frac{2b}{a+b}\right)+C \quad (A.8)$$

where C is an arbitrary constant and F and Π are incomplete elliptic integrals of the first and third kind, respectively.

Proof: Now with the other integral. We start with a simple substitution $2\psi+\pi = \phi'-\phi$ and $2d\psi = d\phi'$:

$$\int \frac{c-d\cos(\phi'-\phi)}{[a-b\cos(\phi'-\phi)]^{3/2}}d\phi' = 2\int \frac{c-d\cos(2\psi+\pi)}{[a-b\cos(2\psi+\pi)]^{3/2}}d\psi$$

We now apply the trigonometric property of the cosine $\cos(2\psi+\pi) = -\cos(2\psi)$:

$$2\int \frac{c-d\cos(2\psi+\pi)}{[a-b\cos(2\psi+\pi)]^{3/2}}d\psi = 2\int \frac{c+d\cos(2\psi)}{[a+b\cos(2\psi)]^{3/2}}d\psi$$

We apply the double angle trigonometric identity and we factor the expressions in the numerator and denominator:

$$2\int \frac{c+d\cos(2\psi)}{[a+b\cos(2\psi)]^{3/2}}d\psi = \frac{2d}{(b)^{3/2}}\int \frac{\frac{c}{d}+1-2\sin^2(\psi)}{\left[\frac{a}{b}+1-2\sin^2(\psi)\right]^{3/2}}d\psi$$

Factoring the expressions the numerator and denominator once again:

$$\frac{2d}{(b)^{3/2}}\int \frac{\frac{c}{d}+1-2\sin^2(\psi)}{\left[\frac{a}{b}+1-2\sin^2(\psi)\right]^{3/2}}d\psi = \frac{2(c+d)}{(a+b)^{3/2}}\int \frac{1-n\,\sin^2(\psi)}{\left[1-m\,\sin^2(\psi)\right]^{3/2}}d\psi$$

Here $m = 2b/(a+b)$ and $n = 2d/(c+d)$. By using Jacobi elliptic functions to make a change of variables in the integral we are able to reduce the integral to a known form. Using the Jacobi elliptic functions, we make a substitution where $\mathrm{sn}(u,m) = \sin(\psi)$, $\mathrm{dn}(u,m) = \sqrt{1-m\sin^2(\psi)}$ and $d\psi/du = \mathrm{dn}(u,m) = \sqrt{1-m\sin^2(\psi)}$. Here $\mathrm{am}(u) = \psi$ and $u = \mathrm{F}(\psi,m)$. We now substitute:

$$\frac{2(c+d)}{(a+b)^{3/2}}\int \frac{1-n\,\sin^2(\psi)}{\left[1-m\,\sin^2(\psi)\right]^{3/2}}d\psi = \frac{2(c+d)}{(a+b)^{3/2}}\int \frac{1-n\,\mathrm{sn}^2(u,m)}{1-m\,\mathrm{sn}^2(u,m)}du$$

Applying the formula (340.01) found in [22] we find the following expression:

$$\frac{2(c+d)}{(a+b)^{3/2}}\int \frac{1-n\,\mathrm{sn}^2(u,m)}{1-m\,\mathrm{sn}^2(u,m)}du$$

$$= \frac{2(c+d)}{m(a+b)^{3/2}}\left[(m-n)\Pi\left(\psi, m, m\right) + n\mathrm{F}\left(\psi, m\right)\right]$$

where C is an arbitrary constant and F and Π are incomplete elliptic integrals of the first and third kind, respectively. By changing variables to the original variables and doing some algebra with the help of Wolfram Mathematica, we obtain the final expression:

$$\begin{aligned}\int \frac{c - d\cos(\phi' - \phi)}{[a - b\cos(\phi' - \phi)]^{3/2}} d\phi' \\ = \frac{2(bc-ad)}{b(a+b)^{3/2}}\Pi\left(\frac{\phi' - \phi - \pi}{2}, \frac{2b}{a+b}, \frac{2b}{a+b}\right) \\ + \frac{2d}{b\sqrt{a+b}}\mathrm{F}\left(\frac{\phi' - \phi - \pi}{2}, \frac{2b}{a+b}\right) + C\end{aligned}$$

ACKNOWLEDGMENT

The authors would like to thank Dr. Sherlie Portugal, a member of the SNI, Panama, for her support during the development of the topics explored in this article.

REFERENCES

[1] A. Kurs, A. Karalis, R. Moffatt, J. D. Joannopoulos, P. Fisher, and M. Soljacic, "Wireless power transfer via strongly coupled magnetic resonances," *Science*, vol. 317, no. 5834, pp. 83–86, Jul. 2007.

[2] P. S. Riehl, A. Satyamoorthy, H. Akram, Y.-C. Yen, J.-C. Yang, B. Juan, C.-M. Lee, F.-C. Lin, V. Muratov, W. Plumb, and P. F. Tustin, "Wireless power systems for mobile devices supporting inductive and resonant operating modes," *IEEE Trans. Microw. Theory Techn.*, vol. 63, no. 3, pp. 780–790, Mar. 2015.

[3] L. Olvitz, D. Vinko, and T. Švedek, "Wireless power transfer for mobile phone charging device," in *Proc. 35th Int. Conv. (MIPRO)*, May 2012, pp. 141–145.

[4] I. Yasar, L. Shi, K. Bai, X. Rong, Y. Liu, and X. Wang, "Mobile phone mid-range wireless charger development via coupled magnetic resonance," in *Proc. IEEE Transp. Electrific. Conf. Expo (ITEC)*, Dearborn, MI, USA, Jun. 2016, pp. 1–8.

[5] F. Musavi, M. Edington, and W. Eberle, "Wireless power transfer: A survey of EV battery charging technologies," in *Proc. IEEE Energy Convers. Congr. Expo. (ECCE)*, Raleigh, NC, USA, Sep. 2012, pp. 1804–1810.

[6] S. Li and C. C. Mi, "Wireless power transfer for electric vehicle applications," *IEEE J. Emerg. Sel. Topics Power Electron.*, vol. 3, no. 1, pp. 4–17, Mar. 2015.

[7] P. Li and R. Bashirullah, "A wireless power interface for rechargeable battery operated medical implants," *IEEE Trans. Circuits Syst. II, Exp. Briefs*, vol. 54, no. 10, pp. 912–916, Oct. 2007.

[8] X. Li, C.-Y. Tsui, and W.-H. Ki, "A 13.56 MHz wireless power transfer system with reconfigurable resonant regulating rectifier and wireless power control for implantable medical devices," *IEEE J. Solid-State Circuits*, vol. 50, no. 4, pp. 978–989, Apr. 2015.

[9] B. J. DeLong, A. Kiourti, and J. L. Volakis, "A radiating near-field patch rectenna for wireless power transfer to medical implants at 2.4 GHz," *IEEE J. Electromagn., RF Microw. Med. Biol.*, vol. 2, no. 1, pp. 64–69, Mar. 2018.

[10] T. M. Hayslett, T. Orekan, and P. Zhang, "Underwater wireless power transfer for ocean system applications," in *Proc. OCEANS MTS/IEEE Monterey*, Monterey, CA, USA, Sep. 2016, pp. 1–6.

[11] D. Shi, L. Zhang, H. Ma, Z. Wang, Y. Wang, and Z. Cui, "Research on wireless power transmission system between satellites," in *Proc. IEEE Wireless Power Transf. Conf. (WPTC)*, Aveiro, Portugal, May 2016, pp. 1–4.

[12] E. M. Purcell, *Electricity and Magnetism*, 3rd ed. Cambridge, U.K.: Cambridge Univ. Press, 2013.

[13] D. J. Griffiths, *Introduction to Electrodynamics*, 4th ed. New York, NY, USA: Cambridge Univ. Press, 2018.

[14] J. D. Jackson, *Classical Electrodynamics*, 3rd ed. New York, NY, USA: Wiley, 1999.

[15] W. R. Smythe, *Static and Dynamic Electricity* (Electromagnetics), 3rd ed. New York, NY, USA: Hemisphere, 1989.

[16] J. V. Bladel, *Electromagnetic Fields* (IEEE Press Series on Electromagnetic Wave Theory), 2nd ed. Hoboken, NJ, USA: IEEE/Wiley-Interscience, 2007.

[17] R. A. Schill, "General relation for the vector magnetic field of a circular current loop: A closer look," *IEEE Trans. Magn.*, vol. 39, no. 2, pp. 961–967, Mar. 2003.

[18] L. Urankar, "Vector potential and magnetic field of current-carrying finite arc segment in analytical form, part I: Filament approximation," *IEEE Trans. Magn.*, vol. 16, no. 5, pp. 1283–1288, Sep. 1980.

[19] L. Urankar, "Vector potential and magnetic field of current-carying finite arc segment in analytical form, part II: Thin sheet approximation," *IEEE Trans. Magn.*, vol. 18, no. 3, pp. 911–917, May 1982.

[20] L. Urankar, "Vector potential and magnetic field of current-carrying finite arc segment in analytical form, part III: Exact computation for rectangular cross section," *IEEE Trans. Magn.*, vol. 18, no. 6, pp. 1860–1867, Nov. 1982.

[21] L. Urankar, "Vector potential and magnetic field of current-carrying finite arc segment in analytical form, part IV: General three-dimensional current density," *IEEE Trans. Magn.*, vol. 20, no. 6, pp. 2145–2150, Nov. 1984.

[22] P. F. Byrd and M. D. Friedman, *Handbook of Elliptic Integrals for Engineers and Scientists*. (Die Grundlehren der mathematischen Wissenschaften 67 in Einzeldarstellungen), 2nd ed. Berlin, Germany: Springer-Verlag, 1971.

[23] M. Igor. *Elliptic Integrals and Functions*. Accessed: Nov. 1, 2020. [Online]. Available: https://www.mathworks.com/matlabcentral/fileexchange/8805-elliptic-integrals-and-functions

MIGDONIO ALBERTO GONZÁLEZ (Member, IEEE) was born in Panama City, Panama, in 1996. He received the engineering degree in electromechanical engineering from the School of Electrical Engineering, Technological University of Panama (UTP), Panama, in 2020. He is currently a Researcher with the Radiant Energy and Irreversible Dissipations (ERDI) Research Group, School of Electrical Engineering. His research interests include theoretical electromagnetics, applied electromagnetics, applied mathematics, and physical simulations.

DORINDO ELÁM CÁRDENAS (Senior Member, IEEE) received the engineering degree in electromechanical engineering from the Technological University of Panama (UTP), Panama, in 2004, and the Ph.D. degree in engineering sciences, with a novel research of mathematical modeling of electrical fires and its sources, that is nominated to the Extraordinary Prize of Doctorate from the Universitat Politècnica de Catalunya–Barcelonatech, Spain, in 2011.

In 2005, he becomes a Professor of electrical engineering at the Technological University of Panama. In 2009, he becomes the Certified Fire Protection Specialist (CFPS), international certification awarded by the National Fire Protection Association (NFPA), USA. In 2014, he was a Postdoctoral Fellow and a Research with The University of Texas at Austin, USA, in radiation transport and variable frequency effects of electromagnetic waves in conductors. He is currently the Main Director of the ERDI Research Group, and a Leader Researcher with the Technological University of Panama. He has been developed professional practice in electrical and mechanical engineering since 2004 to the present in industrial applications. Some of his works include design, installation, and consulting for very large commercial and industrial projects, such as malls, high-rise buildings, power generating plants, electrical substations, and industrial hazardous locations. He has also performed several mathematical modelings for various applications in radiation, energy, chemistry, and other fundamental physical subjects and applied mathematics. He is also a Senior Member of NFPA, IAAI, CFPS, CEMCIT-AIP, and SNI-SENACYT.